

# **Gamma-rays and Neutrinos from Cosmic Accelerators**



# Contents

<b>1</b>	<b>Topics</b>	<b>5</b>
1.1	ICRANet participants . . . . .	5
1.2	Students . . . . .	5
1.3	Ongoing collaborations . . . . .	5
<b>2</b>	<b>Brief description</b>	<b>7</b>
<b>3</b>	<b>Publications-2016</b>	<b>13</b>
3.1	Publications-2010-2015 . . . . .	14
<b>4</b>	<b>Galactic sources of high energy neutrinos: Expectation from gamma-ray data</b>	<b>17</b>
4.1	Introduction . . . . .	17
4.2	The sample . . . . .	18
4.3	Conclusion and Discussion . . . . .	22
<b>5</b>	<b>Gamma-ray Emission from Non-Blazar AGNs</b>	<b>23</b>
5.1	Introduction . . . . .	23
5.2	Fermi-LAT Data Selection and Analysis . . . . .	24
5.3	Results . . . . .	26
5.4	Discussions . . . . .	29
<b>6</b>	<b>High Energy Gamma-Rays From PKS 1441+25</b>	<b>33</b>
6.1	Introduction . . . . .	33
6.2	Fermi-LAT Data Analysis . . . . .	34
6.2.1	Spectral Analysis . . . . .	35
6.3	Discussion and Interpretation . . . . .	38



# 1 Topics

- High energy gamma-ray emission from galactic and extragalactic sources
- Galactic sources of high energy neutrinos

## 1.1 ICRA Net participants

- Aharonian Felix
- Sahakyan Narek

## 1.2 Students

- Zargaryan David
- Baghmany an Vardan
- Karlica Mile
- Gasparyan Sargis

## 1.3 Ongoing collaborations

- Francesco Vissani (INFN, Gran Sasso Theory Group, Italy)
- Frank Rieger (Max-Planck-Institut für Kernphysik, Germany)
- Rui-zhi Yang (Key Laboratory of Dark Matter and Space Astronomy, China)
- Marco Tavani (INAF-IASF Roma and Universit di Roma "Tor Vergata", Italy)
- Paolo Giommi (ASI Science Data Center)
- Ulisses Barres de Almeida (Centro Brasileiro de Pesquisas Físicas - CBPF/MCT)

- Giovanni Piano (INAF-IASF Roma, INFN Roma and Univ. Tor Vergata, Italy)

## 2 Brief description

The works done and currently being developed within our group lie in the field of particle astrophysics including high energy gamma and neutrino astrophysics. The detection of these particles gives the opportunity to understand the physical processes that occur in astrophysical sources: they are not affected by interaction with extragalactic and galactic electromagnetic fields before they reach the Earth, and therefore point directly to the source of emission.

Below we present several abstracts from the papers published in 2015.

- Giant lobes of Centaurus A as seen in radio and  $\gamma$ -ray images obtained with the Fermi-LAT and Planck satellites

The  $\gamma$ -ray data of Fermi-LAT on the giant lobes of Centaurus A are analysed together with the high frequency radio data obtained with the Planck satellite. The large  $\gamma$ -ray photon statistics, accumulated during seven years of observations, and the recently updated Fermi collaboration software tools allow substantial extension of the detected  $\gamma$ -ray emission towards higher energy, up to 30 GeV, and lower energy, down to 60 MeV. Moreover, the new  $\gamma$ -ray data allow us to explore the spatial features of  $\gamma$ -ray emission of the lobes. For the north lobe, we confirm, with higher statistical significance, our earlier finding on the extension of  $\gamma$ -ray emission beyond the radio image. Moreover, the new analysis reveals significant spatial variation of  $\gamma$ -ray spectra from both lobes. On the other hand, the Planck observations at microwave frequencies contain important information on spectra of synchrotron emission in the cutoff region, and thus allow model-independent derivation of the strength of the magnetic field and the distribution of relativistic electrons based on the combined  $\gamma$ -ray and radio data. The interpretation of multi-wavelength spectral energy distributions (SEDs) of the lobes within a pure leptonic model requires strong enhancement of the magnetic field at the edge of the south lobe. Alternatively, a more complex, leptonic-hadronic model of the  $\gamma$ -ray emission, postulating a non-negligible contribution of the  $\pi^0$ -decay component at highest energies, can explain the  $\gamma$ -ray data with a rather homogeneous distribution of the magnetic field over the giant lobes.

- Indication of a local fog of subankle ultrahigh energy cosmic rays

During their propagation through intergalactic space, ultrahigh energy cosmic rays (UHECRs) interact with the background radiation fields. These interactions give rise to energetic electron/positron pairs and photons which in turn feed electromagnetic cascades, contributing to the isotropic gamma-ray background (IGRB). The gamma-ray flux level generated in this way highly depends upon the UHECR propagation distance, as well as the evolution of their sources with redshift. Recently, the *Fermi* collaboration reported that the majority of the total extragalactic gamma-ray flux originates from extragalactic point sources. This posits a stringent upper limit on the IGRB generated via UHECR propagation, and subsequently constrains their abundance in the distant Universe. Focusing on the contribution of UHECR at energies below the ankle within a narrow energy band ( $(1 - 4) \times 10^{18}$  eV), we calculate the diffuse gamma-ray flux generated through UHECR propagation, normalizing the total cosmic ray energy budget in this band to that measured. We find that in order to not over-produce the new IGRB limit, a local “fog” of UHECR produced by nearby sources may exist, with a possible non-negligible contribution from our Galaxy. Following the assumption that a given fraction of the observed IGRB at 820 GeV originates from UHECR, we obtain a constraint on the maximum distance for the majority of their sources. With other unresolved source populations still contaminating the new IGRB limit, and UHECR above the ankle invariably contributing also to this background, the results presented here are rather conservative.

- Radial distribution of the diffuse  $\gamma$ -ray emissivity in the Galactic disk

The Fermi-LAT data accumulated over 7 years of  $\gamma$ -ray observations, together with the high resolution gas (CO & HI) and the dust opacity maps, are used to study the emissivity of  $\gamma$ -rays induced by interactions of cosmic rays (CRs) with the interstellar medium. Based on the dust opacity templates, the  $\gamma$ -ray emissivity was measured for 36 segments of the Galactic plane. Furthermore, the  $\gamma$ -ray emissivity was evaluated in six Galactocentric rings. Both the absolute emissivity and the energy spectra of  $\gamma$ -rays derived in the interval 0.2-100 GeV show significant variations along the galactic plane. The density of CRs, derived under the assumption that  $\gamma$ -rays are predominately produced in CR interactions with the interstellar gas, is characterised by a strong radial dependence. In the inner Galaxy the CR density substantially exceeds the density in the outer parts of the Galaxy: by a factor of a few at 10 GeV, and by more than an order of magnitude at 1 TeV. Remarkably, the energy distribution of CRs appears to be substantially harder than the energy spectrum obtained from direct measurements of local CRs. At the same time, the flux and the energy spectrum of multi-GeV protons derived from  $\gamma$ -ray data in the outskirts of the Galaxy is quite close to the measurements of local CRs.

- 
- Transition of propagation of relativistic particles from the ballistic to the diffusion regime

A stationary distribution function that describes the entire processes of propagation of relativistic particles, including the transition between the ballistic and diffusion regimes, is obtained. The spacial component of the constructed function satisfies to the first two moments of the Boltzmann equation. The angular part of the distribution provides accurate values for the angular moments derived from the Boltzmann equation, and gives a correct expression in the limit of small-angle approximation. Using the derived function, we studied the gamma-ray images produced through the  $pp$  interaction of relativistic particles with gas clouds in the proximity of the accelerator. In general, the morphology and the energy spectra of gamma-rays significantly deviate from the "standard" results corresponding to the propagation of relativistic particles strictly in the diffusion regime.

- Galactic sources of high energy neutrinos: Expectation from gamma-ray data

The recent results from ground based  $\gamma$ -ray detectors (HESS, MAGIC, VERITAS) provide a population of TeV galactic  $\gamma$ -ray sources which are potential sources of High Energy (HE) neutrinos. Since the  $\gamma$ -rays and  $\nu$  -s are produced from decays of neutral and charged pions, the flux of TeV  $\gamma$ -rays can be used to estimate the upper limit of  $\nu$  flux and vice versa; the detectability of  $\nu$  flux implies a minimum flux of the accompanying  $\gamma$ -rays (assuming the internal and the external absorption of  $\gamma$ -rays is negligible). Using this minimum flux, it is possible to find the sources which can be detected with cubic-kilometer telescopes. I will discuss the possibility to detect HE neutrinos from powerful galactic accelerators, such as Supernova Remnants (SNRs) and Pulsar Wind Nebulae (PWNe) and show that likely only RX J1713.7-3946 , RX J0852.0-4622 and Vela X can be detected by current generation of instruments (IceCube and Km3Net). It will be shown also, that galactic binary systems could be promising sources of HE  $\nu$  -s. In particular,  $\nu$  -s and  $\gamma$ -rays from Cygnus X-3 will be discussed during recent gamma-ray activity, showing that in the future such kind of activities could produce detectable flux of HE  $\nu$  -s.

- Gamma-ray Emission from Non-Blazar AGNs

The gamma-ray detection by Fermi-LAT from non blazar active galactic nuclei shows that these are different and potentially very interesting classes of gamma-ray emitters. This provides an alternative approach for studying high energy emission processes compared to blazars where the emission is strongly Doppler boosted. Up to now there are 32 non-blazar AGNs detected

in the gamma-ray band which are included in the third catalog of AGNs detected by Fermi LAT. I will present a detailed investigation of the gamma-ray emission from non-blazar AGNs based on seven years of Fermi LAT data. The accumulation of a larger data set allows detailed temporal analysis in short and long time scales as well as to study the spectrum with better statistics at energies above several GeV. Also the possible origin of observed gamma-rays will be discussed considering both compact and extended regions.

- High Energy Gamma-Rays From PKS 1441+25

In January/April 2015 Fermi-LAT detected strong gamma-ray flares from FSRQ PKS 1441+25 ( $z=0.939$ ). During the flare in January the daily  $\gamma$ -ray flux reached up to  $(1.72 \pm 0.19) \times 10^{-6}$  photon  $\text{cm}^{-2} \text{s}^{-1}$  with the flux double time of  $\approx 1.4$  days. This flare is accompanied by similar flux increase, also in the X-ray band as observed by Swift XRT. The available X-ray and  $\gamma$ -ray data allows to constrain the underlying electron distribution parameters through Markov Chain Monte Carlo method. The emission in the low state can be interpreted by synchrotron self-Compton emission from the electron population producing the radio-to-X-ray emission in the jet while in the high state the emission is mostly produced from inverse-Compton up scattering of the external photons from dusty torus.

- Gamma-Ray Variability of NGC 1275

We present the study of high energy  $\gamma$ -ray emission from NGC 1275 radio galaxy using seven years of public available Fermi-LAT data. The recent upgrade to new Pass 8 event-level analysis (with larger acceptance, a better angular and energy resolution and etc.) allows more detailed temporal and spectral analysis. The light curve with 7-day bins reveals several flaring activities, especially during the last two years of observation, when the weekly flux exceeds the averaged flux nearly 5 times. The flaring activities are investigated by the detected spectrum and temporal analysis. The spectral analysis indicates that in the flaring periods the power-law with exponential cut-off modeling is favored over the simple power-law models. The temporal analysis indicates a day scale variability of flux.

- The Gamma-Ray Emission from Broad-Line Radio Galaxy 3C 120

The results of the analysis of Fermi-LAT data from seven years of observations of the broad line radio galaxy 3C 120 are presented. Compared with the previous studies, now the new PASS 8 data allows to investigate the temporal variability in long and short time scales. The temporal analysis indicates significant variability in short time scales. The spectral analysis is performed for the energies above 100 MeV and high energy  $\gamma$ -rays are detected up to

---

10 GeV. The  $\gamma$ - ray spectrum can be described as synchrotron self-Compton emission from the electron population producing radio-to-X- ray emission in the jet. The required electron energy density exceeds the one of magnetic field, only by a factor of 2.6 meaning no significant deviation from.



## 3 Publications-2016

- A. Prosekin, S. R. Kelner, and F. A. Aharonian, "Polarization of radiation of electrons in highly turbulent magnetic fields", *Physical Review D*, vol. 94, no. 6, 2016.
- X. Sun, R.-z. Yang, B. Mckinley, and F. Aharonian, "Giant lobes of Centaurus A as seen in radio and gamma-ray images obtained with the Fermi-LAT and Planck satellites", *Astronomy and Astrophysics*, vol. 595, 2016.
- L. Ambrogi, E. De Ona Wilhelmi, and F. Aharonian, "On the potential of atmospheric Cherenkov telescope arrays for resolving TeV gamma-ray sources in the Galactic plane", *Astroparticle Physics*, vol. 80, pp. 22-33, 2016.
- R. Liu, A. M. Taylor, X.-Y. Wang, and F. A. Aharonian, "Indication of a local fog of subankle ultrahigh energy cosmic rays", *Physical Review D*, vol. 94, no. 4, 2016.
- F. Voisin, G. Rowell, M. G. Burton, A. Walsh, Y. Fukui, and F. Aharonian, "ISM gas studies towards the TeV PWN HESS J1825-137 and northern region", *Monthly Notices of the Royal Astronomical Society*, vol. 458, no. 3, pp. 2813-2835, 2016.
- R. Yang and F. A. Aharonian, "On the GeV excess in the diffuse gamma-ray emission towards the Galactic centre," *Astrophysics & Astronomy*, vol. 589, 2016.
- R. Yang, F. Aharonian, and C. Evoli, "Radial distribution of the diffuse gamma-ray emissivity in the Galactic disk", *Physical Review D*, vol. 93, no. 12, 2016.
- N. Sahakyan, "Galactic sources of high energy neutrinos: Expectation from gamma-ray data", *EPJ Web of Conferences*, Volume 121, id.05005, 2016.
- N. Sahakyan, V. Baghmanyan, and D. Zargaryan, "Gamma-ray Emission from Non-Blazar AGNs", *AIP proceedings* (2016)

- N. Sahakyan and S. Gasparyan, "High Energy Gamma-Rays From PKS 1441+25", AIP proceedings (2016)
- V. Baghmanyanyan, "Gamma-Ray Variability of NGC 1275", AIP proceedings (2016)
- D. Zargaryan, "The Gamma-Ray Emission from Broad-Line Radio Galaxy 3C 120", AIP proceedings (2016)

### 3.1 Publications-2010-2015

- Kelner, S., Prosekin, A. and Aharonian, F. "Synchro-Curvature Radiation of Charged Particles in the Strong Curved Magnetic Fields", The Astronomical Journal, Volume 149, Issue 1, article id. 33, 21 pp., 2015.
- Bordas, P., Yang, R., Kafexhiu, E. and Aharonian, F. "Detection of Persistent Gamma-Ray Emission Toward SS433/W50", The Astrophysical Journal Letters, Volume 807, Issue 1, article id. L8, 5 pp., 2015.
- Yang, Rui-zhi, Jones, D. and Aharonian, F. "Fermi-LAT observations of the Sagittarius B complex", Astronomy & Astrophysics, Volume 580, id.A90, 7 pp. 2015.
- Sahakyan, N., Zargaryan, D. and Baghmanyanyan, V. "On the gamma-ray emission from 3C 120", Astronomy & Astrophysics, Volume 574, id.A88, 5 pp., 2015.
- Sahakyan, N., Yang, R., Rieger, F., Aharonian, F. and de Ona-Wilhelmi, E. "High Energy Gamma Rays from Centaurus a" Proceedings of the MG13 Meeting on General Relativity ISBN 9789814623995, pp. 1028-1030, 2015.
- Sahakyan, N., Piano, G. and Tavani, M. "Hadronic Gamma-Ray and Neutrino Emission from Cygnus X-3", The Astrophysical Journal, Volume 780, Issue 1, article id. 29, 2014.
- Sahakyan, N., Rieger, F., Aharonian, F., Yang, R., and de Ona-Wilhelmi, E. "On the gamma-ray emission from the core and radio lobes of the radio galaxy Centaurus A", International Journal of Modern Physics: Conference Series, Volume 28, id. 1460182, 2014.
- Sahakyan, N., Yang, R. Aharonian, F. and Rieger, F., " Evidence for a Second Component in the High-energy Core Emission from Centaurus A?", The Astrophysical Journal Letters, Volume 770, Issue 1, L6, 2013.

- Yang, R.-Z., Sahakyan, N., de Ona Wilhelmi, E., Aharonian, F. and Rieger, F., "Deep observation of the giant radio lobes of Centaurus A with the Fermi Large Area Telescope", *Astronomy & Astrophysics*, 542, A19, 2012.
- Sahakyan, N., "High energy gamma-radiation from the core of radio galaxy Centaurus A", *Astrophysics*, 55, 14, 2012.
- Sahakyan, N., "On the Origin of High Energy Gamma-Rays from Giant Radio Lobes Centarus A", *International Journal of Modern Physics Conference Series*, 12, 224, 2012.
- Vissani, F., Aharonian, F. and Sahakyan, N., "On the detectability of high-energy galactic neutrino sources", *Astroparticle Physics*, 34, 778, 2011.



# 4 Galactic sources of high energy neutrinos: Expectation from gamma-ray data

## 4.1 Introduction

The neutrinos are unique messengers which carry astrophysical/cosmological information[1]. Since they can escape from much denser environments (high photon field and/or matter) than  $\gamma$ -rays, it provides a possibility to examine the sources which are impossible by  $\gamma$ -ray detectors. The detection of HE  $\nu$ -s will help to understand the origin of cosmic rays since they are produced in hadronic interactions, thus bring direct information on the hadronic component accelerated in the sources. Many galactic and extragalactic astrophysical object classes are able to accelerate particles above TeV energies which are confirmed by the recent observations with ground based  $\gamma$ -ray detectors (HEGRA, HESS, MAGIC, VERITAS and etc). While the acceleration of leptons (electrons) is limited by relatively short cooling times, the acceleration of hadrons goes beyond TeV/PeV energies. The interaction of these hadrons (with photon fields or matter) produces HE neutrinos ( $> \text{TeV}$ ). Recently, the IceCube detector has detected PeV neutrinos [2], which are probably produced in extragalactic objects (e.g. active galactic nuclei, the source of gamma-ray burst and etc). However, the galactic sources (especially supernova remnants) have been historically considered more favorable sources for HE neutrino detectors. This is justified considering that the galactic sources are responsible for acceleration of cosmic rays at energies below the so-called knee. Perhaps, the chance to detect the first galactic sources will increase with the arrival of KM3Net detector considering the northern hemisphere is more suitable to study galactic sources [3].

Current knowledge on the population and intensity of galactic nonthermal sources (provided by  $\gamma$ -ray detectors) allows to make quantitative estimation on the expectations for HE  $\nu$  detectors. Indeed,  $\gamma$ -rays and neutrinos are produced almost in the same rate in  $pp$  interaction, thus  $\gamma$ -ray data can be used as a guide for neutrino searches. In [3], it was shown that the most relevant energy range for  $\gamma$ -ray observations (which will provide one event in neu-

trino detector) is around 20 TeV, where the intensity of  $\gamma$ -ray is at the narrow range of  $I_\gamma \sim (2 - 6) \times 10^{-15} \text{ TeV}^{-1} \text{ cm}^{-2} \text{ s}^{-1}$  [3]. However, for now only limited data are available at 20 TeV, which will be highly explored with the future planned CTA instrument, therefore we try to obtain a limit at somewhat lower energies which are currently better investigated (e.g.  $\sim 1$  TeV).

Let's suppose accelerated protons interact with low energy protons ( $pp$  interaction) and produce  $\gamma$ -rays. If the source is transparent for produced  $\gamma$ -rays, one can derive a limit on the  $\gamma$ -ray flux which accompanying HE  $\nu$  flux can be detected by current instruments. The sensitivity of nowadays HE  $\nu$  detectors (e.g. IceCube) at 1 TeV are:

$$F_{sens}(E_\nu = 1 \text{ TeV}) = \begin{cases} 1.7 \times 10^{-11} \text{ TeV}^{-1} \text{ cm}^{-2} \text{ s}^{-1} & \text{-- after 1 year} \\ 4.9 \times 10^{-12} \text{ TeV}^{-1} \text{ cm}^{-2} \text{ s}^{-1} & \text{-- after 5 years} \end{cases} \quad (4.1.1)$$

On the other hand, the ratio between  $\gamma$ -ray and  $\nu$  fluxes produced in  $pp$  interaction for broad proton distribution ( $dN_p/dE_p \sim E_p^{-\alpha}$ ,  $\alpha = (1.5 \div 3.5)$ ) corresponds to:  $\frac{F_\gamma}{F_\nu} \approx (0.6 - 2.5)$  (see Fig. 2 in [4]). Taking into account this ratio and assuming that the HE  $\nu$  flux corresponds to the threshold value presented in Eq. 4.1.1, it can be calculated the corresponding  $\gamma$ -ray luminosity for a given distance ( $d$ ). This luminosity corresponds to:

$$L_\gamma(E_\gamma = 1 \text{ TeV}) = \begin{cases} (1.95 \div 8.13) \times 10^{33} \left(\frac{d}{1 \text{ kpc}}\right)^2 \text{ erg s}^{-1} & \text{-- after 1 year} \\ (5.6 \div 23.3) \times 10^{32} \left(\frac{d}{1 \text{ kpc}}\right)^2 \text{ erg s}^{-1} & \text{-- after 5 years} \end{cases} \quad (4.1.2)$$

A  $\gamma$ -ray source can be also detected by current  $\nu$  detectors, if at the distance  $d = 1$  kpc it has a  $\gamma$ -ray luminosity exceeding the limits presented in the Eq. 4.1.2. Accordingly, measuring the  $\gamma$ -ray flux at 1 TeV (and a corresponding luminosity) by comparing with the values presented in Eq. 4.1.2 we can find relevant sources for observations with HE  $\nu$  detectors. The limit presented in Eq. 4.1.2 was obtained assuming the source is transparent for produced  $\gamma$ -rays. The absorption of the  $\gamma$ -rays introduces uncertainties, between  $\gamma$ -ray and  $\nu$  fluxes and the limits presented in Eq. 4.1.2 are not applied anymore. In particular, such conditions are satisfied for galactic binary systems which we discuss separately.

## 4.2 The sample

In principle above mentioned limits can be applied for both galactic and extragalactic sources. Poor understanding of physics of extragalactic sources (e.g. AGN and GRBs) and intrinsic and/or intergalactic absorption hard-

ens the prediction for extragalactic objects. Instead, the situation is more clear with the galactic sources: comparatively better information on physical processes responsible for  $\gamma$ -ray and  $\nu$  emissions. The recent observations in GeV/TeV band clearly demonstrated that several classes of galactic sources, such as supernova remnants, pulsar wind nebulae and microquasars (binary systems), are effective particle accelerators above TeV energies. However, in some cases both leptonic and hadronic scenarios can successfully reproduce the observed HE  $\gamma$ -ray data. Without going into details, here we assume that the observed  $\gamma$ -rays have a hadronic origin and we discuss the perspectives of detecting HE neutrinos from these sources.

All the results from observations in HE energy band (including all instruments) are listed in *TeVCat*. Currently it contains around 150 sources which include both galactic and extragalactic objects. We consider only sources belonging to SNRs and PWNe classes, which are powerful nonthermal emitters up to very high energies.

**Supernova Remnants:** SNRs were considered as the main sources of galactic cosmic rays after the arguments by Baade and Zwicky in 1934 [5]. A modest efficiency of  $\sim 10\%$  in converting the kinetic energy of supernova shocks into particle acceleration and the rate of SNRs in our Galaxy can explain the observed flux of cosmic rays. There was no observation proof of proton acceleration in SNRs shock until recently, since both leptonic and hadronic modelings give a satisfactory description of the  $\gamma$ -ray data. However, recently AGILE and Fermi-LAT measured pion bumps in SNRs IC 443 and W 44 [6, 7, 8] which show indirect evidence of the acceleration of hadronic particles in SNRs. If so, it is natural to consider SNRs as potential targets for HE  $\nu$  observations.

Currently, there are 10 SNRs interacting with molecular clouds and 13 shell type SNRs which are listed in *TeVCat*. Unfortunately, for some sources there are missing measurements of flux at 1 TeV (e.g. photon index) and only 20 SNRs are included in the sample. We assume, that the  $\gamma$ -rays have pure hadronic origin and we compare the luminosity at 1 TeV with limits obtained in Eq. 4.1.2. Fig. 4.1 (on the left) illustrates the luminosity of shell type SNRs (circle) and SNRs interacting with molecular clouds (square) compared with the  $\gamma$ -ray luminosity. The filled area corresponds to different initial proton distributions changing from very soft  $\alpha = 3.5$ -long dashed to very hard  $\alpha = 1.5$ -dashed (solid line represents the power-law index  $\alpha = 2$ ). As one can see, most of sources have  $\gamma$ -ray flux nearly two order of magnitude below than required threshold. It appears only for two powerful SNRs, the measured  $\gamma$ -ray luminosity is in the order of presented limit. These are SNRs RX J1713.7-3946 and RX J0852.0-4622 which have been extensively discussed as potential targets for HE  $\nu$  detectors. Different estimations show that in principle several events in a year exposure can be detected if the produced  $\gamma$ -rays

## 4 Galactic sources of high energy neutrinos: Expectation from gamma-ray data

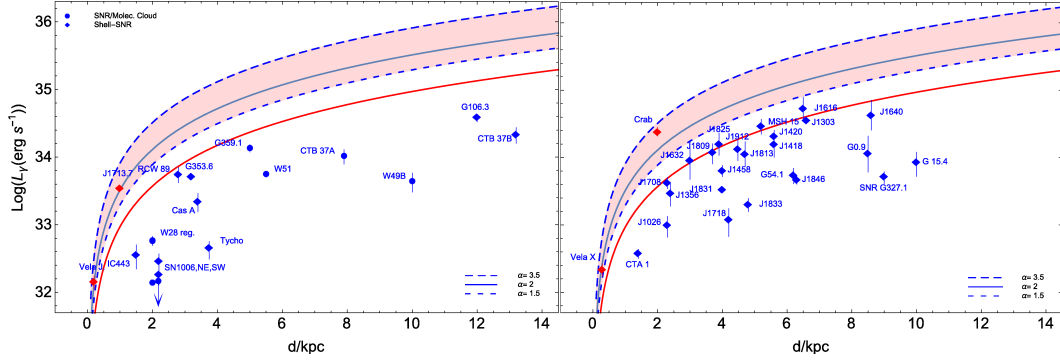


**Figure 4.1:** Gamma-ray luminosity of SNRs (on the left) and PWNe (on the right) compared with the minimal  $\gamma$ -ray luminosity required to produce detectable HE  $\nu$  flux. The filled area corresponds to different power-law indicis of initial protons ( $\alpha = (1.5 \div 3.5)$ ).

have hadronic origin (however, up to now the leptonic origin can not be disfavored). The location of these two SNRs is not covered by IceCube, but they are perfect targets for future planned KM3Net instrument.

The red solid line in Fig. 4.1 corresponds to necessary  $\gamma$ -ray luminosity in order to detect HE  $\nu$ -s after 5-years of observations. It is noticeable, that even in this case the situation is not improved: only above mentioned SNRs will be detected. The  $\gamma$ -ray observations should find new SNRs otherwise the expectations from currently known SNRs are not promising.

**Pulsar wind nebulae:** PWNe are another class of galactic sources which accelerate particles up to VHEs. If one assumes the fraction of accelerated particles are protons, then from the inelastic interactions between accelerated protons and the ambient gas HE/VHE  $\gamma$ -rays and  $\nu$ -s are produced. Of course, the presence of bayronic component in pulsar winds (coexisting) with the leptonic one is still an open question and moreover the pulsar must efficiently convert rotational energy into proton acceleration. However, considering the difficulties with the leptonic modeling, the hadronic scenario remains attractive for  $\gamma$ -ray emission from PWNe. This makes PWNe another class of galactic sources producing HE  $\nu$ -s.

The number of PWNe detected in TeV band and presented in *TeVCat* corresponds to 35 but for 7 sources no data are available. For remaining 28 sources, we assume that the produced  $\gamma$ -rays have pure hadronic origin and compare with the limits presented in Eq. 4.1.2 (see Fig. 4.1). Similar to the previous case, the luminosity of almost all sources is significantly below than the required limit and only two sources, Crab nebulae and Vela X, have flux satisfying mentioned limit. One of these sources, crab nebulae - a very well studied object in all wavelengths, emits  $\gamma$ -rays up to TeV band which are most likely

produced from inverse Compton scattering of soft photon fields inside the nebula. In case if  $\gamma$ -rays are produced from protons, from this source also HE  $\nu$  can be detected. However, so far no evidence for proton contribution seen from the observations. On the other hand, Vela X PWN, an active pulsar (PSR B0833-45) associated with nebula, can be easily detectable with the current instrument ( $\gamma$ -ray flux corresponds to  $L_\gamma \sim 1.7 \times 10^{32} \text{ erg s}^{-1}$  exceeding the obtained limits). The origin of unusual TeV  $\gamma$ -rays (photon index  $\Gamma \approx 1.32$ ) [9] is under debates but considering the difficulties for modeling within leptonic scenarios, the hadronic origin can not be disfavored. All this arguments show that Vela region (Vela X PWN and Vela Junior SNR) is a prime candidate for galactic  $\nu$  sources to be detected with KM3Net.

It should be noted, that after 5-years of exposure, some of the sources can be detected with current HE  $\nu$  instruments (red solid line in Fig. 4.1). Compared with the previous case, this is improved, but still few events in 5-years of observations do not make these source potentially interesting for  $\nu$  astronomy.

*Binary systems:* For a long time, binary systems were considered as potential  $\gamma$ -ray emitters, however unavoidable absorption of HE  $\gamma$ -rays (by optical photons in the systems) makes hard their detection. The improved sensitivity of current instruments results the detection of GeV/TeV  $\gamma$ -rays from binary systems (microquasars) confirmed that their emission extends up to TeV energies (or even higher energies). If the  $\gamma$ -rays are produced from protons, the flux of HE  $\nu$  -s can significantly exceed the one of  $\gamma$ -rays (by a factor of  $e^\tau$  where  $\tau$  is the optical depth) considering that they escape from the region without absorption unlike the  $\gamma$ -rays. Due to the unknown parameter  $\tau$  no acceptable limit can be drawn in this case. However, below it is demonstrated that using the observed  $\gamma$ -ray flux from Cygnus X-3 (well known galactic microquasar) and under reasonable assumptions for absorption it can be detected by neutrino detectors.

It has been shown, that  $\gamma$ -ray flaring activity from microquasar Cygnus X-3 can be well explained within hadronic scenario [10]: protons accelerated via jet interact with the wind particles from companion Wolf-Rayet star. Normalizing the proton spectrum using AGILE data (unabsorbed) and taking into account the absorption above GeV energies (in order not to overcome MAGIC upper limits) the expected HE  $\nu$  flux is only by a factor of about 3 lower than the 1-year IceCube sensitivity at  $\sim 10$  TeV. Considering a prolonged "soft X-ray state" (which is characterized by  $\gamma$ -ray emission), the  $\nu$  flux from this source might be close to being detectable by cubic-kilometer  $\nu$  telescopes such as IceCube. Moreover, the estimations for HE  $\nu$  -s from another galactic binary system, LS 5039, show that the flux of HE  $\nu$  -s can be as large as  $1.6 \times 10^{-11} \text{ cm}^{-2} \text{ s}^{-1}$  (for energy greater than 1 TeV) [11], above the sensitivity threshold of experiments in the Mediterranean Sea (KM3Net). This shows that probably binary systems are a class of galactic objects, from

which the first galactic HE  $\nu$  -s will be detected.

### 4.3 Conclusion and Discussion

The cubic kilometer scale HE  $\nu$  detectors with the existing HE  $\gamma$ -ray detectors provide an opportunity to study nonthermal processes in both galactic and extragalactic objects in great detail. While the recent detection of PeV  $\nu$  by IceCube demonstrate the beginning of extragalactic  $\nu$  astronomy, the first galactic sources of HE  $\nu$  still have to be detected. There are several classes of galactic sources, which *i*) can accelerate the particles (hadrons) up to hundreds of TeV energies and *ii*) are established to be TeV emitters. Clearly, the first galactic source which will be detected, belongs to one of these well established classes of TeV emitters.

The flux of TeV  $\gamma$ -ray allows to estimate the expected flux of HE  $\nu$  , if the  $\gamma$ -rays have a hadronic origin and produced  $\gamma$ -rays do not suffer from absorption in the sources. Indeed, the minimal detectable flux of HE  $\nu$  implies the minimal flux of accompanying  $\gamma$ -rays . Such estimation shows, that from already detected SNRs and PWNe, only two SNRs, RX J1713.7-3946 and RX J0852.0-4622, one PWN- Vela X, have significantly high HE  $\nu$  flux, which can be detected with current  $\nu$  detectors. Even longer exposure time (5-years) will not significantly increase the number of potentially detectable sources. However, if the  $\gamma$ -rays from above mentioned sources have a hadronic origin they will provide several events in kilometer-cube scale size detector in a year exposure.

On the other hand, the unexpected high flux of HE  $\nu$  -s can be detected from galactic binary systems (recently established strong TeV emitters). The effective absorption of TeV  $\gamma$ -rays , means that the flux of HE  $\nu$  can exceed the  $\gamma$ -ray one by several orders of magnitude (depending on the optical depth  $\tau$ ). The estimation of HE  $\nu$  flux from several binary systems (e.g., Cygnus X-3, LS 5039) shows that it is either in the same order or exceeds the sensitivity of the current instruments. Moreover, considering that the TeV  $\gamma$ -rays can be totally absorbed in the system (high density of soft photons), the  $\nu$  observations might discover new binary systems which are not "seen" by  $\gamma$ -ray instruments. Therefore, these are the best targets for HE  $\nu$  detectors.

# 5 Gamma-ray Emission from Non-Blazar AGNs

## 5.1 Introduction

The recent results from the observations in MeV/GeV band constitute that the largest population of extragalactic  $\gamma$ -ray sources are Active Galactic Nucleus (AGNs) with a jet pointed at a small angle to the line of sight. The radiation from these sources (called blazars) is strongly amplified by Doppler boosting: the observed flux is related to the rest-frame flux by  $F(\nu) \sim \delta^3 F(\nu')$  where  $\nu'$  is the emitted photon frequency in the rest frame.  $\gamma$ -ray emission from blazars shows strong variability (minutes and day-scales) which means that the radiation is produced in sup-pc scales and it is a unique possibility to investigate jet structures in parsec or sub-parsec scales. At the same time, the emission from extended regions (e.g., knots, lobes [12] and etc) which is not boosted remains invisible. In principle, these regions which contain valuable information regarding the jet particle density, jet acceleration power etc, can be investigated considering AGNs with a larger inclination angle (e.g. Radio Galaxies (RG)). Thus the observations of these misdirected AGNs provide different approaches to study high energy processes in AGNs.

After four years of all sky monitoring with Fermi Large Area Telescope (*Fermi* LAT), 26 RGs of different types have been reported as GeV  $\gamma$ -ray emitters [28]. Although, the small number of detected objects makes the population study difficult, the results of individual objects contain important information about the high energy properties of these objects.  $\gamma$ -ray emission from both Fanaroff and Riley type-I (FRI) and type-II RGs have been detected. Following the Fanaroff and Riley classification [14], FRI sources have surface brightness that is larger toward their cores, while for FR II sources, the brightening increases toward the edges. The jet of low power FRI sources appears to be relatively inefficient at transporting energy, while the high-power sources, FR IIs, have fast, efficient jets. Probably the accretion in the FRI sources is relatively inefficient while most FR IIs have an efficient engine and a dusty torus. Up to now 10 FR Is, 3-FR IIs, 7- Soft-Spectrum Radio Quasars (SSRQs) and 1 - Compact Steep-Spectrum Quasar (CSS) have been detected in the  $\gamma$ -ray band and are included in the third catalog of AGNs detected by the *Fermi* LAT [28].

SSRQs have characteristics more similar to FR II and jet inclination angle between these of FSRQs and FR IIs. Instead, CSS radio sources are small ( $< 1$  kpc) in size but are morphologically similar to kpc-Mpc double-sided radio galaxies. In addition, to these sources, we include also 3C 120 which recently has been detected in the  $\gamma$ -ray band [15]. The source Fornax A is included in the sample but the recent analysis indicates that  $\gamma$ -ray emission from this particular source is produced in the extended lobes [16].

Prior to the launch of the Fermi satellite, only the RG and blazar sub-class of AGNs have been detected in the  $\gamma$ -ray band. However, the recent results indicated that also Narrow Line Seyfert 1 (NLSy1) galaxies are potential sources of  $\gamma$ -rays. NLSy1 are AGNs with optical spectral properties similar to those of Seyfert 1 galaxies, except for having narrow Balmer lines and strong optical  $F_e$  II lines [17]. NLSy1 exhibit strong X-ray variability, steep X-ray spectra, relatively high luminosity, and substantial soft X-ray excess [18]. These characteristics point to systems with smaller masses of the central black hole ( $10^6 - 10^8 M_\odot$ ) than blazars and radio galaxies, and higher accretion rates (close to or above the Eddington limit). Up to now, already 5 NLSy1s have been detected in the  $\gamma$ -ray band which have interesting temporal and spectral properties in the  $\gamma$ -ray band.

Our sample, in total, contains 28 objects from 3 different sub-classes of AGNs. The investigation of the origin of  $\gamma$ -ray emission from these objects based on the 7-year of Fermi LAT data will allow detailed investigation of particle acceleration and emission processes in the RGs.

## 5.2 Fermi-LAT Data Selection and Analysis

Large Area Telescope, on board the Fermi satellite is a pair-conversion telescope sensitive to  $\gamma$ -rays in the energy range between 20 MeV - 300 GeV [31]. Most of the time, it constantly scans the whole sky already more than 8 years (operating since August 4, 2008) which allows to investigate the  $\gamma$ -ray sky over a long time period.

Here we use publicly available data accumulated during 7 years of Fermi LAT operation, between 4th August 2008 and 4th August 2015 corresponding to the Mission Elapsed Time (MET) interval of 239557417– 460339204. The data were analyzed with standard Fermi Science Tools v10r0p5 software package released on May 18 2015, available from the Fermi Science Support Center <sup>1</sup>. The latest reprocessed Pass 8 events with energy between 90 MeV and 310 GeV and spacecraft data are used with the instrument response function P8R2\_SOURCE\_V6 and enabling energy dispersion correction. How-

---

<sup>1</sup><http://fermi.gsfc.nasa.gov/ssc/data/analysis/software/>

ever, the likelihood analysis was restricted to 100 MeV - 300 GeV energy interval. Only events with higher probability of being photons (`evclass=128` `evtype=3`) are analyzed. Standard cuts (e.g., the zenith angle larger than  $90^\circ$ ) are applied to reduce Earth limb  $\gamma$ -rays (produced from the interaction of cosmic rays with atmosphere).

The photons were downloaded from  $10^\circ$  around each source position taken from [32] (except for 3C 207, M87, PKS 1502+036, PKS 2004-447 and 1 H 0323+342, the radius  $12^\circ$  is chosen to have better modeling of the region of interest (ROI)) and worked with a  $14^\circ \times 14^\circ$  square ROI. The photons are binned with `gtbin` tool with a stereographic projection into pixels of  $0.1^\circ \times 0.1^\circ$  and into 35 equal logarithmically-spaced energy bins. The model file is created using the *Fermi* LAT third source catalog [32] (3FGL) where all sources within ROI+ $5^\circ$  region were included in the model file. For the Galactic and diffuse background models `gll_iem_v05_rev1` and `iso_source_v05` are used, currently recommended by LAT team. The normalization of background models as well as fluxes and spectral indices of the sources within ROI are left as free parameters in the analysis. In order to find the best matches between spectral models and events, the binned likelihood analysis is performed with `gtlike` and the detection significance is quantitatively estimated using the Test Statistics (TS), defined as  $TS = 2(\log L - \log L_0)$ , where  $L$  and  $L_0$  are the likelihoods with an additional source and null hypothesis [33].

Using data from longer accumulation time than used in 3 FGL, can result new  $\gamma$ -ray sources in the ROI which are not properly accounted in the model files. In order to probe for additional sources, a TS significance map of the ROI is created using the best-fit model. After subtracting the observed counts from the model map (constructed with the resulting likelihood model), if there are new sources with  $TS > 25$  they are included in the source model file during data analysis, in addition to the 3FGL sources.

In the spectral analysis, initially the source spectra were modeled using Power-Law (PL) spectral shape. In case, the source spectra shows deviation from simple PL modeling, more complex Power-Law with Exponential cut-off (PLEXP) or log parabolic (LP) shapes are considered. In order to check for statistically significant curvature in the spectrum, log likelihood ratio test was performed. After the likelihood fitting in the energy range between 0.1-300 GeV, the Spectral Energy Distribution (SED) of each source has been obtained by dividing the total interval into smaller bands and separately running `gtlike` for these intervals.

In order to quantify the variability within 7 years, the total observational time has been divided into shorter time periods. Then, with a `gtlike` tool, the unbinned likelihood analysis is performed restricting the (0.1 – 300) GeV energy range with appropriate quality cuts applied as in the previous case. In the model file, the photon indices of all sources are fixed to the best guess

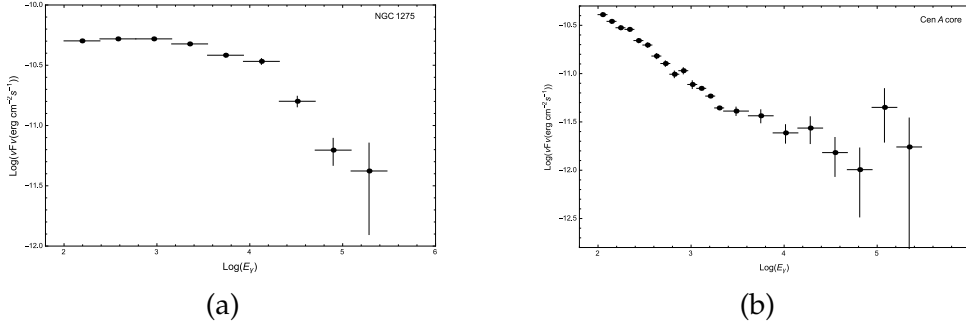


**Figure 5.1:** SEDs of NGC 1275 and Cen A core for the energy range from 100 MeV to 300 GeV.

values to reduce uncertainties in the flux estimation. Since the variability is not expected for underlying background diffuse emission, we fixed the best-fit parameters as to the average values obtained from the 7-year integrated spectrum for Galactic/extragalactic background components.

The possible variation is investigated in both short and long time scales. For some sources, pure statistics do not allow to investigate the variability shorter than a 6-month period while for bright source the light curves with denser time sampling are investigated. The minimal time interval used in the light curves generation has been chosen so that the period when the source has been detected by *Fermi* LAT corresponds to the large fraction of total bins. To search if the variability is present a  $\chi^2$  test will be performed.

### 5.3 Results

The results from the current data analysis are summarized in the Table 6.1. For each source the class,  $\gamma$ -ray photon index ( $\Gamma$ ), flux ( $F_\gamma$ ), distance ( $d$ ),  $\gamma$ -ray luminosity ( $L_\gamma(\text{erg s}^{-1})$ ) and TS are presented. Since reprocessed PASS 8 version of data is used, most of sources have been detected well above  $5\sigma$  limit which allowed to investigate the source spectrum above 1 GeV energies which is crucial for testing the break or turn-over in the spectrum.

The results presented here are consistent with those reported in [28] but with reduced uncertainties in the flux and photon index due to the collection of longer data set resulting to the improved photon statistics. Only the source TXS 0348+013 initially included in the sample of non-blazar AGNs [28] appeared with detection significance below  $5\sigma$  limit (TS 14) thus we did not include it in the Table 6.1. The highest detection significance corresponds to  $\sim 267\sigma$  for NGC 1275 while the 3C 303 has been detected almost at the threshold limit  $5.1\sigma$ . The observed lower photon flux corresponds to

$1.49 \times 10^{-9}$  photon  $\text{cm}^{-2} \text{s}^{-1}$  for 3C 303 at the same time the brightest sources have photon flux in the order of few times  $10^{-7}$  photon  $\text{cm}^{-2} \text{s}^{-1}$  (e.g., Cen A, NGC 1275).

The  $\gamma$ -ray spectrum of most of the sources is well represented with PL model. However, the spectrum of several sources appears with curvature or with turn-over and more complex models are required. For example, in the Fig. 1 the SED of NGC 1275 is depicted, which shows curvature in the spectrum (steepening above 10 GeV) and PLEXP spectrum better explains the observed data. Similar steepening is observed also in the spectrum of NGC 6251 albeit the spectrum starts to drop above 1 GeV energies. The source PKS 0625-31 has relatively hard spectrum  $\Gamma \sim 1.86$  and the emission extends up to  $> 100$  GeV energies. Even if a steepening above (30 – 40) GeV is noticeable a PLEXP representation of the data is not statistically significant to reject the simple PL modeling. However, the recent detection of the source above 250 GeV with H.E.S.S. instrument with the photon index  $2.8 \pm 0.5$  [22] strengthens the assumption about the break in the  $\gamma$ -ray emission spectrum. The  $\gamma$ -ray emission from the core of Cen A RG appears with interesting modification. Indeed, in the previous works it has been already illustrated that the  $\gamma$ -ray spectrum appears with unusual break around 4 GeV [23]. Now, with the new data the spectrum of Cen A can be investigated with better statistics and a break with high confidence level ( $5\sigma$ ) around 3 GeV is found when the spectrum hardens from 2.7 to 2.3 (Fig. 1 (b)). Interestingly, the extrapolation of the component with photon index 2.3 to the TeV energies can satisfactorily reproduce the data in the TeV band from the H.E.S.S observations [24] showing that the emission in these bands is produced from the same component. This can be additional evidence that different components are forming the Cen A spectrum in the 100 MeV- 3 TeV energy range.

In principle, the observed  $\gamma$ -rays can be produced both in compact and extended regions. The localization of  $\gamma$ -ray emission from both RGs and blazars is still an open problem. However variability, if present, could provide important constraints on the emitting region size. An observed flux variation on timescale  $t_{\text{var}}$ , for example, would limit the (intrinsic) size of the  $\gamma$ -ray production region to  $R \leq \frac{\delta_d}{z+1} c t_{\text{var}}$ , where  $\delta$  is the Doppler factor and  $z$  is the redshift. Therefore the variability will allow to distinguish between the extended and compact emitting regions.

The previous variability studies did not reveal significant variability of the RGs in the  $\gamma$ -ray band and only the emission from NGC 1275 was characterized by temporal and spectral variability [25]. The new data analysis indicates that among FRI/FR II sources, in addition to NGC 1275 also the emission from 3C 380 and 4C +39.23B appears with temporal variability. The  $\gamma$ -ray light curves of NGC 1275 and 3C 380 are depicted in Fig. 2 with 7-day and 2-

month time intervals. The  $\chi^2$  test shows highly variable flux where the probability that the flux is constant is below  $10^{-3}$ . In addition, similar test applied to the light curve of 4C +39.23B with 6-month bins shows  $\chi^2/\text{dof} \approx 2.2$  with the probability  $p(\chi^2) = 0.01$  which is consistent with variability. It should be mentioned that  $\chi^2$  analysis of the monthly light curve of M87 and PKS 0625-35 indicates possible variability, however, because of limited statistics no definite conclusion can be drawn. From non variable sources Cen B and NGC 6251, which have high detection significance ( $18\sigma$  and  $32\sigma$  respectively) are particularly important since the extended lobes of these sources have been already considered as possible sites where  $\gamma$ -rays are produced. Now, the absence of statistically significant variability indirectly supports the assumption that  $\gamma$ -rays are produced in the extended regions. The pure statistics did not allow the investigation of the variability for the rest of considered sources in a time period with a year (or sometimes 6-months) binning which does not allow to make definite conclusions regarding the variability.

The high photon statistics from the observations of NLSy1 sources allowed

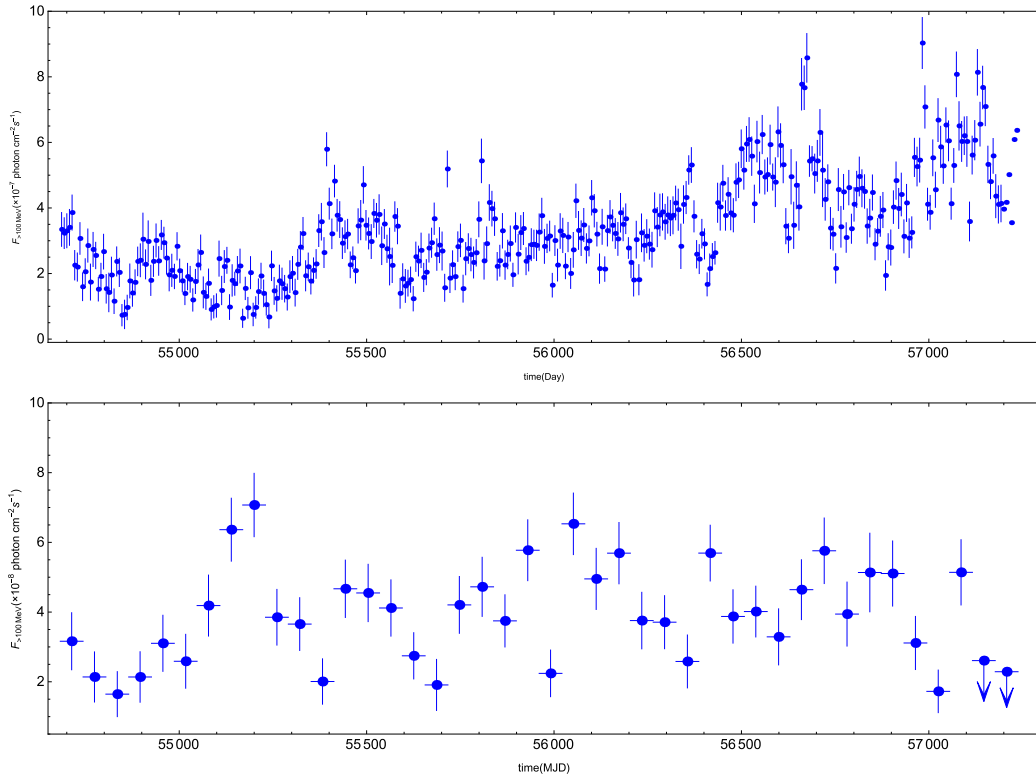


**Figure 5.2:** The  $\gamma$ -ray light curves of NGC 1275 (upper) and 3C 380(lower).

detailed investigation of the  $\gamma$ -ray flux variability. The  $\gamma$ -ray emission from SBS 0846+513, 1H 0323+342, PMN J0948+0022 is strongly variably in sub-

month time scales showing several bright flaring periods. For example, the light curve of SBS 0846+513 with 15-day binning indicates the flux increased nearly 9 times from its averaged level and also the photon index modified from 2.24 to 2.0 during June - July 2011. Interestingly, during the next significant  $\gamma$ -ray flux brightening (August 2012), the flux increased only by its intensity but the photon index remained almost the same (2.24). This indicates that perhaps the physical origin of these flares is different. The other two NLSy1 sources (PKS 1502+036 and PKS 2004-447) show variability in month time scales with no significant flaring periods. The detailed investigation of the variability of NLSy1 sources will be investigated in the future works.

## 5.4 Discussions

We have studied the  $\gamma$ -ray emission from non-blazar AGNs included in the third catalog of AGNs detected by the *Fermi* LAT using the 7-year of *Fermi* LAT accumulated data. The sample consists from 12 FR I, 3 FR II, 6 SSRQ, 1 CSS and 5 NLSy1 and we have found the following main results.

*i)* The number of detected FR I and FR II are nearly the same considering SSRQ and CSS are FR II sources. Each class is characterized by different photon indexes which ranges from  $\Gamma = 1.8$  to  $\Gamma = 2.8$ . The sources with harder photon indexes are PKS 0625-35 and TXS 0331+3915 ( $\Gamma \approx 1.8$ , both are FR I) while the FR II sources appear with softer photon index ( $\Gamma > 2.3$ ). This difference in photon indexes is connected with different radiative cooling suffered by the relativistic electrons in jets propagating in different ambients, e.g. due to the strong radiative cooling in FR II sources the electrons appear with smaller energies. Moreover FR I and FR II sources are characterized by different luminosities: FR Is have lower  $\gamma$ -ray luminosity (the maximum observed luminosity is  $2.2 \times 10^{44}$  erg s $^{-1}$  for NGC 1275) whereas FR IIs have luminosity which can reach up to few times  $10^{46}$  erg s $^{-1}$ . In the photon index luminosity plan the NLSy1 sources have similar characteristics with FR II one which is connected with the fact that *i)* the jets of NLSy1 have inclination angle smaller than FR I sources more similar to SSRQs and *ii)* the jet propagates in the medium with reach photon fields similar to FR IIs. The powerfull FR II and NLSy1 sources are detected even at a larger distance with the most distant source 4C +39.23B at the redshift  $z = 1.21$ .

*ii)* The spectral analysis indicates that PL spectral model gives a good representation of the Table 6.1 sources SED. However, deviation from simple power-law modeling is observed in the individual source spectra. Namely, PLEXP spectral model can explain the steeping observed in the spectra of NGC 1275 and NGC 6251 assuming the break at the energies  $\approx 30$  GeV and 7.2 GeV, respectively. The modeling of PKS 0625-35 spectrum with PLEXP

spectrum statistically is not preferred over simple PL modeling but there is an indication of steepening of the spectrum. The modeling of Cen A core spectrum with broken power-law modeling confirmed the break around  $\approx 3$  GeV when the spectrum hardens from 2.7 to 2.8.

*iii)*The temporal analysis indicates new variable sources among FRI/FRII sources in addition to the previously reported variability of NGC 1275. The sources 3C 380, 4C +39.23B and Cen A core (low energy component) show clear variability in month time scales whereas some indication of variability is present in the light curves of M87 and PKS 0625-35. The light curve of NGC 1275 is one of the most interesting one which shows a complex structure with several flaring periods when the flux increases several times from its average level. The fit of flare structures indicates minimum folding time in the order of 7 days indicating the emission is produced in the compact emitting region. Moreover, statistically significant flux brightenings during the short time periods are observed in the light curve of 3C 120 and 3C 111. For example, during the week between 21-27 September 2014 and 20-26 April 2015, the  $\gamma$ -ray fluxes of 3C 120 increased nearly 10 times and the photon index was changed from 2.69 to 2.25. Among, the NLSy1 sources SBS 0846+513, 1H 0323+342, PMN J0948+0022 are characterized by sub-month time scale variability while the month time scale variability is present in the light curves of PKS 1502+036 and PKS 2004-447.

**Table 5.1:** Results of the Fermi-LAT Data Analysis

Source Name	$\Gamma$	$F_\gamma(> 90 \text{ MeV})$	$d(\text{cm})$	$L_\gamma(\text{erg s}^{-1})$	TS
3C 264	$1.99 \pm 0.15$	$2.93 \pm 1.24 \times 10^{-9}$	$2.83 \times 10^{26}$	$3.5 \times 10^{42}$	78.5
NGC 1275	$2.01 \pm 0.14$	$3.75 \pm 0.03 \times 10^{-7}$	$2.29 \times 10^{26}$	$2.2 \times 10^{44}$	71118
3C 120	$2.69 \pm 0.06$	$4.11 \pm 0.55 \times 10^{-8}$	$4.3 \times 10^{26}$	$3.35 \times 10^{43}$	332.4
Cen A Core	$2.66 \pm 0.02$	$1.94 \pm 0.06 \times 10^{-7}$	$1.17 \times 10^{25}$	$1.19 \times 10^{41}$	6107
NGC 2484	$2.11 \pm 0.01$	$2.09 \pm 0.06 \times 10^{-9}$	$5.58 \times 10^{26}$	$7 \times 10^{42}$	28.03
Cen B	$2.47 \pm 0.05$	$7.36 \pm 0.87 \times 10^{-8}$	$1.69 \times 10^{25}$	$1.23 \times 10^{41}$	341.79
M87	$2.02 \pm 0.04$	$1.84 \pm 0.18 \times 10^{-9}$	$5.68 \times 10^{25}$	$8.18 \times 10^{41}$	1033.52
NGC 6251	$2.35 \pm 0.03$	$2.81 \pm 0.15 \times 10^{-8}$	$3.26 \times 10^{26}$	$2 \times 10^{43}$	1001
NGC 1218	$2.03 \pm 0.08$	$7.15 \pm 1.58 \times 10^{-9}$	$3.73 \times 10^{26}$	$1.32 \times 10^{43}$	178.8
TXS 0331+3915	$1.84 \pm 0.17$	$1.59 \pm 0.1 \times 10^{-9}$	$2.68 \times 10^{26}$	$2.91 \times 10^{42}$	41.8
PKS 0625-35	$1.87 \pm 0.04$	$1.18 \pm 0.12 \times 10^{-8}$	$7.1 \times 10^{26}$	$1.35 \times 10^{44}$	915.7
Fornax A	$2.32 \pm 0.08$	$1.12 \pm 0.16 \times 10^{-8}$	$5.74 \times 10^{25}$	$2.55 \times 10^{41}$	181.5
3C 111	$2.70 \pm 0.05$	$4.87 \pm 0.32 \times 10^{-8}$	$6.32 \times 10^{26}$	$8.2 \times 10^{43}$	254.75
3C 303	$2.02 \pm 0.19$	$1.49 \pm 0.8 \times 10^{-9}$	$1.84 \times 10^{27}$	$7.16 \times 10^{43}$	26.0
Pictor A	$2.53 \pm 0.12$	$1.38 \pm 0.37 \times 10^{-8}$	$4.57 \times 10^{26}$	$1.48 \times 10^{43}$	118.66
3C 207	$2.63 \pm 0.08$	$1.58 \pm 0.23 \times 10^{-8}$	$8.69 \times 10^{27}$	$5.69 \times 10^{45}$	120.8
3C 221	$2.41 \pm 0.09$	$9.65 \pm 1.75 \times 10^{-9}$	–	–	120
3C 275.1	$2.47 \pm 0.12$	$1.1 \pm 0.24 \times 10^{-8}$	$7.23 \times 10^{23}$	$3.12 \times 10^{45}$	106
3C 380	$2.43 \pm 0.03$	$4.35 \pm 0.22 \times 10^{-8}$	$9 \times 10^{27}$	$2.04 \times 10^{46}$	1328
PKS 1203+04	$2.69 \pm 0.17$	$8.45 \pm 2.5 \times 10^{-9}$	$8.19 \times 10^{27}$	$2.55 \times 10^{45}$	31.08
4C +39.23B	$2.46 \pm 0.06$	$2.13 \pm 0.23 \times 10^{-8}$	$1.58 \times 10^{28}$	$3.12 \times 10^{45}$	413
3C 286	$2.71 \pm 0.14$	$1.08 \pm 0.25 \times 10^{-8}$	$1.11 \times 10^{28}$	$5.61 \times 10^{45}$	63
SBS 0846+513	$2.24 \pm 0.02$	$4.63 \pm 0.18 \times 10^{-8}$	$7.62 \times 10^{27}$	$2.15 \times 10^{45}$	3129
1H 0323+342	$2.83 \pm 0.03$	$8.93 \pm 0.33 \times 10^{-8}$	$7.95 \times 10^{26}$	$2.28 \times 10^{44}$	1405
PMN J0948+0022	$2.627 \pm 0.02$	$1.61 \pm 0.17 \times 10^{-7}$	$7.62 \times 10^{27}$	$4.27 \times 10^{46}$	6346
PKS 1502+036	$2.631 \pm 0.04$	$5.27 \pm 0.28 \times 10^{-8}$	$5.31 \times 10^{27}$	$6.88 \times 10^{45}$	933
PKS 2004-447	$2.629 \pm 0.06$	$2.91 \pm 0.26 \times 10^{-8}$	$3.13 \times 10^{27}$	$1.32 \times 10^{45}$	351

1 2



# 6 High Energy Gamma-Rays From PKS 1441+25

## 6.1 Introduction

Blazars are an extreme class of Active Galactic Nuclei (AGNs) which have jets that are forming small angle with respect to the line of sight [27]. Blazars are known to emit electromagnetic waves in almost all frequencies that are currently being observed, extending from radio to  $\gamma$ -ray bands. Since the blazar jet has small inclination angle, the emitted radiation will appear brighter towards the observer due to the relativistic beaming. Typically, the matter in the blazars' jet moves with velocities close to the speed of light (large bulk factor) thus the beaming factor can become very large ( $\delta \sim (10 - 20)$ ) which implies the emitted luminosity is significantly amplified (by  $\sim \delta^4$  times). The main feature of the non-thermal blazar emission is a distinct variability at all frequencies with different variability time scales ranging from years down to a few minutes. The shortest variability time scales are usually observed for the highest energy band, for example minute scale variability of PKS 2155-304 [26] which implies the emission is produced in a very compact region. Therefore, the observation of blazars is a unique chance to investigate the jet structure in sub-parsec scales.

Commonly, the blazars are divided into BL Lacertae (BL-Lac) objects and Flat-Spectrum Radio Quasars (FSRQs) where BL-Lacs show no sign of emission lines, whereas the FSRQs are more distant, more luminous, and have stronger emission lines [27]. In the unified models of AGNs, it is believed that radio galaxies (AGNs with larger inclination angle) are the parent population of blazars, namely the FSRQs are associated with FR II radio sources, while the BL-Lac objects with low luminous FR I sources. Considering the environments where the jet propagates in BL-Lacs and FSRQs are different, the cooling of relativistic electrons will be different, thus those classes will be characterized by different photon indexes. Indeed, the FSRQs, which have very reach and effective nuclear region (thus the electrons effectively loss energy) are found to be soft, while BL Lacs represent on average a population of harder-spectrum sources [28]. Therefore, the particle acceleration and emission processes in those sources are different and the investigation of radiation

mechanisms provides different views of High Energy (HE;  $> 100$  MeV) processes.

HE observations of blazars are especially important, considering the photons with these energies are produced from particles accelerated up to hundreds of TeV energies which allow us to investigate the particle accelerations in the most extreme regimes. Also, the Extragalactic Background Light (EBL) intensity can be estimated using the absorption of Very High Energy (VHE;  $> 100$  GeV) photons by the interaction with EBL photons.

In the VHE  $\gamma$ -ray band the majority of detected blazars is BL-Lac objects, in particular those with the synchrotron bump peaking in the UV/X-ray band. Particularly, it is interesting the detection of VHE photons from blazars belonging to the FSRQs class, since the broad line region structure of those objects, which is rich in optical-UV photons, makes these environments strongly opaque to  $\gamma$ -rays and the detection of those objects in the VHE  $\gamma$ -ray band is rather surprising.

Recently, HE and VHE  $\gamma$ -rays are detected from the distant blazar PKS 1441+25 ( $z=0.939$ ) with VERITAS [29] and MAGIC [30] instruments. This illustrates that some of the radiated photons escape pair production interaction with both EBL photons and the radiation near the black hole, and suggested that the emission region is located beyond the BLR region. The  $\gamma$ -ray light curve of PKS 1441+25 shows several prominent flaring activities which are accompanied by flux increase also in the X-ray band. In the current work, the underlying particle distribution of the flare, observed in January 2015, is investigated using the data from Fermi-LAT and Swift XRT.

## 6.2 Fermi-LAT Data Analysis

Large Area Telescope, on board the Fermi satellite (Fermi-LAT) is a pair-conversion telescope sensitive to  $\gamma$ -rays in the energy range 20 MeV - 300 GeV. It constantly scans the whole sky every 3 hours already more than 8 years which allows to investigate  $\gamma$ -ray sky over a long time period. More details about Fermi-LAT instrument can be found in [31].

In the present paper we use publicly available data accumulated during 6-28 January simultaneous with Swift XRT observations (which corresponds to the Mission Elapsed Time (MET) interval of 442195203– 444096003). The data were analyzed with standard Fermi Science Tools v10r0p5 software package released on May 18 2015, available from the Fermi Science Support Center <sup>1</sup>. The latest reprocessed Pass 8 events spacecraft data are used with the instrument response function P8R2\_SOURCE\_V6 . We downloaded photons

---

<sup>1</sup><http://fermi.gsfc.nasa.gov/ssc/data/analysis/software/>

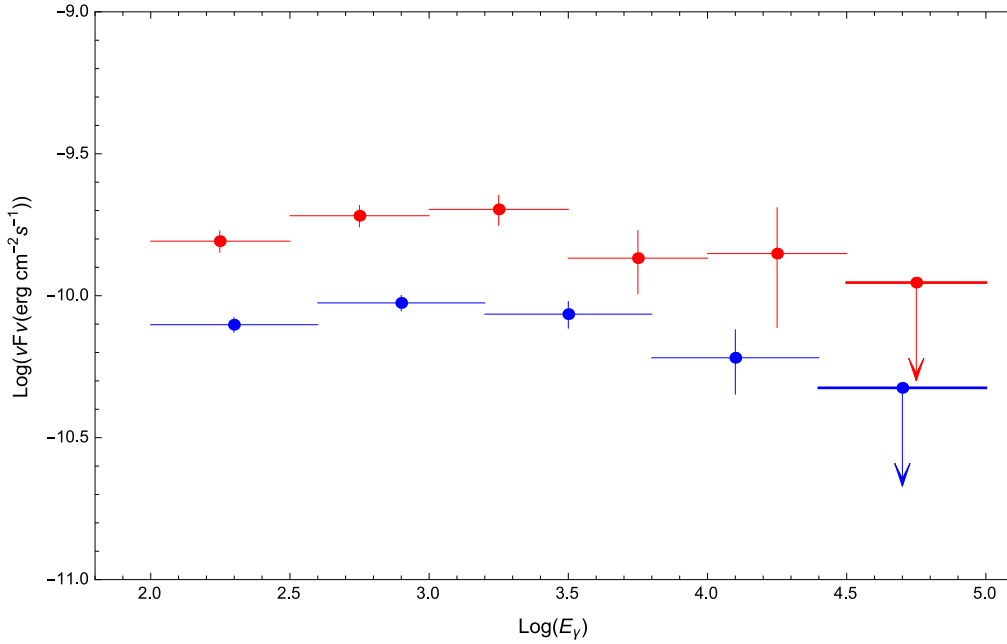


**Figure 6.1:** The  $\gamma$ -ray Spectral Energy Distribution (SED) of PKS 1441+25 averaged over Fermi-LAT observations in January 2015 (blue data). SED obtained during the flaring period between 21-28 January is depicted with red colors.

in the energy range 100 MeV-100 GeV from a region of interest defined as a circle of 20 deg radius centered at the position of PKS 1441+25 (RA, Dec) = (220.996, 25.039). During the analysis only events with higher probability of being photons (evclass=128 evtype=3) are analyzed. A cut on zenith angle  $90^\circ$  was applied to reduce contamination from Earth-limb  $\gamma$ -rays, produced by cosmic rays interacting with the upper atmosphere. The model file describing the region of interest contains point sources from Fermi-LAT third source catalog [32] within 25 deg from the target, as well as Galactic *gll\_iem\_v05\_rev1* and isotropic *iso\_source\_v05* diffuse components. All point-source spectra were modeled with the same spectral model used in the catalog, allowing the photon index and normalization of the sources within 20 deg to be free in the analysis. Also, the normalization of diffuse-background components were not fixed.

### 6.2.1 Spectral Analysis

In order to find the best matches between spectral models and events, an unbinned likelihood analysis is performed with *gtlike*. Initially the spectrum of PKS 1441+25 is modeled assuming a power-law, considering the normaliza-

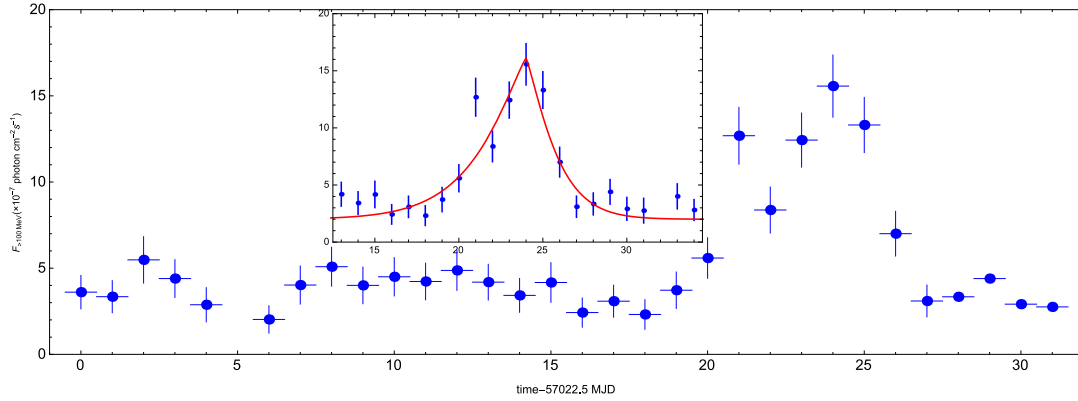


**Figure 6.2:** Light curve of  $0.1 < E_\gamma < 100$  GeV  $\gamma$ -rays from PKS 1441+25 during January 2015. The bin intervals correspond to 1- days. The flare fit with the Eq. 6.2.4 is highlighted in the small plot.

tion and power-law index as free parameters. The best fit spectrum obtained with *gtlike* corresponds to:

$$\left(\frac{dN}{dE}\right)_p = (3.03 \pm 0.17) \times 10^{-11} \left(\frac{E}{1406.7 \text{ MeV}}\right)^{-1.99 \pm 0.04}. \quad (6.2.1)$$

yielding an integral flux of

$$F_\gamma(> 100 \text{ MeV}) = (5.89 \pm 0.3) \times 10^{-7} \text{ photon cm}^{-2} \text{ s}^{-1}, \quad (6.2.2)$$

with only statistical errors taken into account. The source detection significance quantified by Test Statistics (TS), defined as  $TS = 2(\log L - \log L_0)$  [33], where  $L$  and  $L_0$  are the likelihoods with an additional source and null hypothesis, corresponds to  $TS = 2174$  above 100 MeV, which is equal to  $\approx 46.6 \sigma$  detection significance. Figure 6.1 shows the spectrum of PKS 1441+25 obtained by separately running *gtlike* for 5 energy bands equal in a log scale.

The lightcurve of PKS 1441+25 was constructed by applying the above analysis method to a day-time bins. Then, with *gtlike* tool the unbinned likelihood analysis is performed restricting (0.1 – 100) GeV energy range with appropriate quality cuts applied as in the previous case. In the model file, the photon indices of all other sources are fixed to the best guess values to reduce uncertainties in the flux estimation and the photon index of PKS 1441+25 and normalization of all sources within 20 deg are considered as free parameters.

The  $\gamma$ -ray lightcurve of the PKS 1441+25 obtained with the one-day binning is presented in Fig. 6.2. A major flaring period is clearly visible. Bright flaring peak is evident around 25 January with the daily averaged flux of  $(1.72 \pm 0.19) \times 10^{-6} \text{ photon cm}^{-2} \text{ s}^{-1}$ . During the flaring period the photon

index corresponds to  $\Gamma = 1.95$ , thus it was not changed significantly. The flux increase is observed around 21 January and it lasts up to 28 January.

In order to investigate the flaring period, the  $\gamma$ -ray data accumulated in the period between 21-28 January 2015 are analyzed. The best fit parameters describing the spectrum obtained from the unbinned analysis with *gtlike* are:

$$\left(\frac{dN}{dE}\right)_p = (5.59 \pm 0.38) \times 10^{-11} \left(\frac{E}{1406.7 \text{ MeV}}\right)^{-1.968 \pm 0.04} \quad (6.2.3)$$

which corresponds to  $F_\gamma(> 100 \text{ MeV}) = (1.05 \pm 0.06) \times 10^{-6} \text{ photon cm}^{-2}\text{s}^{-1}$  flux and the predicted photon counts from PKS 1441+25 are  $N_{\text{pred}} = 517.2$ . The Fig. 6.1 shows Fermi-LAT spectrum of PKS 1441+25 obtained by separately running *gtlike* for 6 bins (red) where a deviation from power-law modeling above  $\sim 3 \text{ GeV}$  is noticeable. An alternative fit of power-law with exponential cutoff function in the form  $dN/dE \sim E_\gamma^{-\alpha} \times \text{Exp}(-E_\gamma/E_{\text{cut}})$  is performed, which results to  $\alpha = 1.81$  and  $E_{\text{cut}} = 12 \pm 5.2 \text{ GeV}$ . In order to compare the power-law and the power-law with exponential cutoff models, a log likelihood ratio test between the models is applied. The TS is twice the difference in these log likelihoods, which gives 8 for this case. Note that the probability distribution of the TS can be approximated by a  $\chi^2$  distribution with 1 dof, corresponding to the difference of dof between two functions. The results give  $P(\chi^2) = 0.0046$  which again indicates a deviation from a simple power-law function.

To derive the timescales of the flare, the light curve is fitted with a two-sided exponential function in the form of

$$\begin{aligned} F(t) &= F_c + F_0 \times \text{Exp}\left[-\left(\frac{|t-t_0|}{\sigma_r}\right)^k\right] \\ &= F_c + F_0 \times \text{Exp}\left[-\left(\frac{|t-t_0|}{\sigma_d}\right)^k\right] \end{aligned} \quad (6.2.4)$$

where  $t_0$  is the time of the maximum intensity of the flare ( $F_0$ ),  $F_c$  represents the constant level present in the flare,  $\sigma_r$  and  $\sigma_d$  are the rise ( $t < t_0$ ) and decay ( $t > t_0$ ) time constants, respectively, and  $k$  is a measure of the flare sharpness. The time of maximum flare has been fixed during the fitting procedure and the other parameters are considered as free parameters. The fit results in  $F_0 = (14 \pm 2.2) \times 10^{-7} \text{ photon cm}^{-2}\text{s}^{-1}$ ,  $\sigma_r = 3.15 \pm 0.7$ ,  $\sigma_d = 1.95 \pm 0.4$  and  $k = 1.19 \pm 0.3$ . Using this technique, it is also possible to estimate the shortest time variability which is defined by  $\tau = \sigma \times (\ln 2)^{(1/k)}$  and corresponds to  $\tau_d = 1.4 \text{ d}$ . This illustrates that there is a doubling of flux in 1.4 d-scales which will allow to constrain the emitting region size.

### 6.3 Discussion and Interpretation

Usually, the SED of a blazar consists of two broad non-thermal radiation components in different energy domains. The first component, ranging from radio to optical or X-ray energies, is usually attributed to synchrotron radiation of relativistic electrons interacting with ambient magnetic fields. The origin of the HE spectral component, covering the X-ray to  $\gamma$ -ray regime, is still under debate. It can be modeled by the inverse Compton radiation coming from low-energy photon fields that interact with the relativistic electrons [34]. This process can be described either by a Synchrotron-Self Compton (SSC) model, where the electrons scatter their self-generated synchrotron photons [35], or by so-called external Compton models (EC), where the seed photons are generated in the accretion disk [36], the broad-line region [37], or the dusty torus [38] of the central black hole. The exact localization of  $\gamma$ -ray emission region is still an open problem and it is unclear which external photon field dominates.

The simultaneous multiwavelength data from the observations of PKS 1441+25 are depicted in the Fig. 6.3. In the low state, the archival data are from ASI Science Data Center collected in different periods. The X-ray data in the high period are from [29] and  $\gamma$ -ray data are from two different epoch times: blue points simultaneous with Swift XRT (January) observations and red points in the flaring period between 21-28 January (January-flare).

In order to model the emission in the low and high states SSC and EC models are considered. In the synchrotron/SSC modeling, it is assumed the emission comes from a spherical region with the radius  $R_b$  moving with Lorentz factor  $\Gamma = (1 - \beta)^{-1/2}$ . The size of the emitting region can be constrained from 1.4 d variability of HE  $\gamma$ -ray flux which implies the emission is produced from a region with a size smaller than  $< 1/(1+z)\tau c \delta \sim 1.87 \times 10^{16} (\delta/10)$  cm. The emission is boosted by  $\delta = 1/[\Gamma(1 - \beta \cos(\theta))]$  where  $\theta$  is the angle between the bulk velocity and the line of sight. For the Doppler beaming  $\delta = 10$  and  $\delta = 18$  are considered for low and high states respectively. The observations of PKS 1441+25 in April 2015 with MAGIC and VERITAS instruments show that the emission is produced in a region beyond the broad line region. Thus, the photons from dusty torus are the main field for external photons. For the torus, we assume luminosity  $L_{\text{torus}} = 0.6 L_{\text{disk}}$  [39] where  $L_{\text{disk}} \approx 2 \times 10^{45} \text{ erg s}^{-1}$  is inferred from the luminosity of broad line region [40] and temperature  $T \approx 10^3 \text{ K}$ .

The underlying electron distribution is assumed to have power-law with exponential cutoff  $\left(\frac{dN}{dE}\right)_{PLEC} = N_0 \gamma^{-\alpha} \text{Exp}\left(-\left(\frac{\gamma}{\gamma_c}\right)\right)$  or broken power-law form  $\left(\frac{dN}{dE}\right)_{BPL} = N_0 \gamma^{\alpha_1}$  if  $\gamma \leq \gamma_{br}$  and  $\left(\frac{dN}{dE}\right)_{BPL} = N_0 \gamma_{br}^{\alpha_2 - \alpha_1} \gamma^{-\alpha_2}$  if  $\gamma > \gamma_{br}$ . The parameters giving the best description of the data are obtained with a

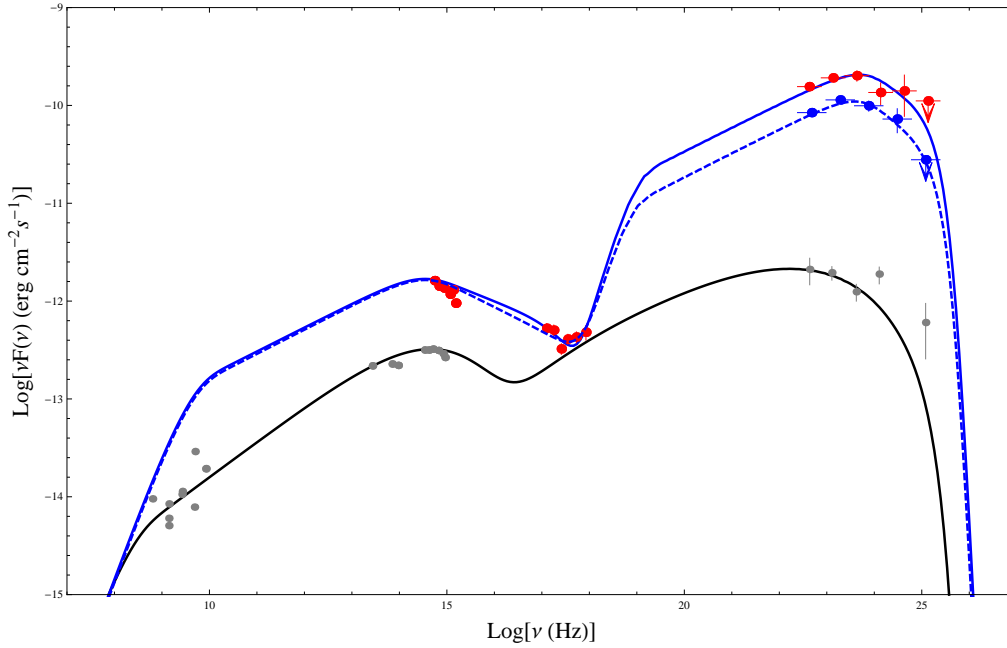


**Figure 6.3:** Multiwavelength emission of PKS 1441+25 considering SSC and EC models. The blue line corresponds to the modeling in the flaring period while the dashed line for the period simultaneous with Swift XRT observations. The EBL absorption is included in the model calculations.

publicly available *naima* package [41], which can derive the best-fit and uncertainty distributions of spectral model parameters through Markov Chain Monte Carlo (MCMC) sampling of their likelihood distributions. The prior likelihood, our prior knowledge of the probability distribution of a given model parameter and data likelihood functions, are passed onto the emcee sampler function for an affine-invariant MCMC run. In addition, there are multiple simultaneous walkers, which improve the efficiency of the sampling and reduce the number of computationally-expensive likelihood calls. In the modeling, the synchrotron, and IC radiative models included in the *naima* package are used. The electron synchrotron emission is computed for a random magnetic field, according to the approximation provided in [42]. This approximation provides better than 0.2 % accuracy over the entire range of energy. The full Klein-Nishina cross section is used in the calculation of the IC scattering using the kelner from [43], and both synchrotron and torus photon fields are considered. We run the sampling with 64 simultaneous walkers, for 100 steps of burn-in, and 100 steps of run. In the parameter sampling, the following expected ranges are considered:  $1.5 \leq (\alpha, \alpha_1, \alpha_2) \leq 10$  and  $1 \text{ GeV} \leq E_{c,br} \leq 1 \text{ TeV}$ ,  $0.511 \text{ MeV} \leq E_{\min} \leq 1 \text{ TeV}$  and  $0.511 \text{ MeV} \leq E_{\max} \leq 1 \text{ TeV}$ .

The results are depicted in the Fig. 6.3, while the corresponding parameters

**Table 6.1:** Parameters for the models presented in Fig. 6.2.4.

Parameters	Low	January	January-Flare
$N_0^2$	$910 \pm 42$	$502.2 \pm 227$	$944.3 \pm 360$
$\alpha_1$	$2.275 \pm 0.01$	$2.50 \pm 0.08$	$2.511 \pm 0.06$
$\alpha_2$	–	$3.48 \pm 0.03$	$3.385 \pm 0.06$
$E_{\min}(\text{MeV})$	$3.288 \pm 2.22$	$6.36 \pm 0.67$	$7.4 \pm 0.6$
$E_{c,br}(\text{GeV})$	$7.42 \pm 0.42$	$2.03 \pm 0.17$	$2.22 \pm 0.19$
$E_{\max}(\text{GeV})$	$162.6 \pm 40$	$92.18 \pm 12.4$	$71.5 \pm 8.4$
$B(\text{G})$	$0.124 \pm 0.007$	$0.321 \pm 0.016$	$0.235 \pm 0.01$

are presented in Table 6.1. In the low state power-law with exponential cutoff electron distribution gives a better representation of the data while the broken power-law spectral model is preferred for the modeling in the high state. The maximum electron energy  $E_{\max}$  is estimated using the X-ray data for the high periods but in the low state the X-ray data are missing, thus it is defined by the  $\gamma$ -ray data. The estimations show that in the flaring period it is in the order of  $E_{\max} = (70 - 90)$  GeV. The power-law slop is characterized with the index order of  $\sim 2.5$  before the break which steepens to  $\sim 3.5$  at the break energies  $\approx 2$  GeV. The obtained magnetic field strength ( $\sim 0.3$  G) is in the limit for the similar parameters estimated for the blazars. The modeling allows to estimate the particle and magnetic field energy content in the jet. The equipartition condition is significantly violated in the low state  $U_e/U_B \approx 3880$  while there is no large deviation in the flaring periods ( $U_e/U_B \approx 16$  for January and  $U_e/U_B \approx 50$  for January flare).

In the future works, also the flaring event observed in April of 2015 will be investigated applying a similar technique. The comparison of the underlying electron distribution properties in two different flaring periods with the low state will allow to understand the origin of the observed flares.

# Bibliography

- [1] Aharonian, F., Nuclear Physics B Proceedings Supplements, **221**, 5 (2011)
- [2] Aartsen, M. G. et al, Phys. Rev. Lett., **111**, 021103 (2013)
- [3] Vissani, F. Aharonian, F. and Sahakyan, N., Astroparticle Phys., **34**,10, p. 778-783, 1 (2013)
- [4] Kelner, S., Aharonian, F. and Bugayov, V., Phys. Rev. D, **74**, 3, id. 034018 (2006)
- [5] Baade, W. and Zwicky, F. Proceedings of the National Academy of Science, **20**, 259 (1934).
- [6] Giuliani, A., Cardillo, M. et al, ApJL, **742**, 2, L30, 5 pp. (2011).
- [7] Tavani, M., Giuliani, A. et al, ApJ, **710**, 2, L151 (2010).
- [8] Ackermann, M., Ajello, M. et al, Science, **339**, 6121, 807-811 (2013).
- [9] Abramowski, A., Acero, F. et al, A& A, **548**, A38, 11 (2012).
- [10] Sahakyan, N., Piano, G. and Tavani, M., ApJ, **780**,1, 29, 7 (2014).
- [11] Aharonian, F. et al, JPCS, **39**, 1, 408 (2006).
- [12] R.Z. Yang, N. Sahakyan et al., A&A 542, A19 (2012)
- [13] M. Ackermann, M. Ajello et al., ApJ 810, 14 (2015)
- [14] B. Fanaroff and J. Riley, MNRAS 167, 31P (1974)
- [15] N. Sahakyan, D. zargaryan et al., A&A 574, A88 (2015)
- [16] M. Ackermann, M. Ajello et al., ApJ 826, 1 (2016)
- [17] D. Osterbrock and R. Pogge, ApJ 297, 166 (1985)
- [18] L. Gallo, MNRAS 368, 479 (2006)
- [19] W. Atwood, A. Abdo et al., ApJ 697, 1017 (2009)

- [20] P. Nolan, A. Abdo et al., *ApJ* 199, 2012
- [21] J. Mattox and D. Bertsch et al., *ApJ* 461, 396 (1996)
- [22] M. Dyrda, A. Wierzcholska et al., *ArXiv e-prints*, 1509.06851 (2012)
- [23] N. Sahakyan, R. Yang et al., *ApJL* 770, L6 (2013)
- [24] F. Aharonian, A. Akhperjanian et al., *ApJ* 695, L40 (2009)
- [25] J. Kataoka, L. Stawarz et al., *ApJ* 740, 29 (2011)
- [26] F. Aharonian, A. Akhperjanian et al., *ApJ* 664, 71 (2007)
- [27] M. Urry and P. Padovani, *PASP* 107, 803 (1995)
- [28] M. Ackermann, M. Ajello et al., *ApJ* 810, 14 (2015)
- [29] A. Abeysekara, S. Archambault, et al., *ApJL* 815, L22 (2015)
- [30] L. Ahnen, S. Ansoldi, et al., *ApJL* 815, L23 (2015)
- [31] W. Atwood, A. Abdo et al., *ApJ* 697, 1017 (2009)
- [32] P. Nolan, A. Abdo et al., *ApJ* 199 (2012)
- [33] J. Mattox and D. Bertsch et al., *ApJ* 461, 396 (1996)
- [34] M. Böttcher M., *ASS* 309, 95 (2007)
- [35] G. Ghisellini, L. Maraschi, and A. Treves, *A&A*, 146, 204 (1985)
- [36] C. Dermer, R. Schlickeiser, *ApJ* 416, 458 (1993)
- [37] M. Sikora, M. Begerlman and M. Rees, *ApJ* 421, 153 (1994)
- [38] M. Blazejowski, M. Sikora, R. Moderski, G. Madejski, *ApJ* 545, 107 (2000).
- [39] G. Ghisellini, L. Maraschi, F. Tavecchio, *MNRAS* 396L, 105 (2009)
- [40] R. Xiong and X. Zhang, *MNRAS* 441, 3375 (2014)
- [41] V. Zabalza, *Proc. of International Cosmic Ray Conference* (2015)
- [42] F. Aharonian, S. Kelner, and A. Prosekin, *PRD* 82, 4 (2010)
- [43] F. Aharonian and A. Atoyan, *APSS* 79, 321 (1981)